Biosensors and Bioelectronics xxx (xxxx) 114707

Contents lists available at ScienceDirect

Biosensors and Bioelectronics

journal homepage: www.elsevier.com/locate/bios

Spoon-shaped polymer waveguides to excite multiple plasmonic phenomena: A multisensor based on antibody and molecularly imprinted nanoparticles to detect albumin concentrations over eight orders of magnitude

Nunzio Cennamo [a], Francesco Arcadio [a], Mimimorena Seggio [b], Devid Maniglio [c], Luigi Zeni [a], Alessandra Maria Bossi [b, *]

[a] University of Campania Luigi Vanvitelli, Department of Engineering, Via Roma 29, 81031, Aversa, Italy
[b] University of Verona, Department of Biotechnology, Strada Le Grazie 15, 37134, Verona, Italy
[c] University of Trento, Department of Industrial Engineering, Via Sommarive 9, 38123, Trento, Italy

ARTICLE INFO

Keywords:
Polymeric multimode waveguide sensors
Spoon-shaped waveguides
Surface plasmon resonance (SPR)
Immunosensor
Molecularly imprinted polymers
nanoMIPs sensor

ABSTRACT

A polymeric multimode waveguide, characterized by a pioneering spoon-shaped geometry, was herein proposed for the first time to devise Surface Plasmon Resonance (SPR) biochemical sensors. The plasmon excitation was enabled by layering a gold nanofilm of ~60 nm onto the spoon-waveguide. As a consequence of the waveguide's extra-ordinary geometry, two distinct sensing regions were identified: a planar one, located on the spoon's neck, and a concave one on the bowl, with angled surfaces. The bulk sensitivity (S_n) is correlated both to the way the light was launched in/collected from the sensor (parallel or orthogonal to the main axis of the waveguide) and to the sensing area interrogated (planar-neck or angled-bowl), indicating that the sensor's performance can be conveniently tuned, depending on the chosen measuring configuration. The SPR sensor's characterization showed S_n equal to 750 nm/RIU for the neck and to 950 nm/RIU for the bowl. To further inspect the peculiar sensing-features and assess the application niches, the spoon-shaped waveguide was functionalized with two kinds of receptors, both specific for human serum albumin (HSA): an antibody on the bowl region (high S_n); molecularly imprinted nanoparticles (nanoMIPs) on the neck region (low S_n). The experimental results showed a limit of detection (LOD) for the immune-sensor of 280 pM and an LOD for the nanoMIP-sensor of 4.16 fM. The overall response of the HSA multi-sensor encompassed eight orders of magnitude, suggesting that the spoon-shaped waveguide's provides multi-scale detection and holds potential to devise multi-analyte sensing platforms.

1. Introduction

Plasmonics has become a dominant technique for diverse fields of applications, from chemical/biological sensing to process monitoring in chemical and pharmaceutical industries, environmental engineering and modern super-resolution imaging (Chatterjee et al., 2021; Mejía-Salazar et al., 2018). Plasmonic sensors have notably high sensitivity, real-time responses, low-costs, the possibility of remote interrogation and the label-free analysis, which make them ideal for the detection of biological targets, such as bacteria, viruses, and protein biomarkers. The Surface Plasmon Resonance phenomenon at the basis of plasmonic sensing exploits the interaction of light with the target analyte to be sensed at the interface between a metal (e.g. a gold film) and a dielectric. It results in an absorption phenomenon that is extremely sensitive to the changes in the refractive index (RI) of the dielectric medium close to the metal. SPR is extensively used as operating principle in biosensors, achieving low nanomolar to picomolar detection ranges (Homola, J. 2003; Nguyen et al., 2015; Singh, P. 2016; Tong et al., 2014). SPR excitation is effectively obtained by the optical configuration proposed by Kretschmann-Raether in 1968 (Kretschmann E., 1971; Kretschmann and Raether, 1968), indeed this has long prevailed in the development of SPR devices. However, from the years 2000, optical waveguides, like optical fibers made of plastic, glass or specialty ones, have been increasingly preferred to excite the SPR. Waveguides offer several advantages, like the passive nature, electromagnetic immunity, small size, remote sensing capabilities, low-cost and chemical stability

* Corresponding author.
E-mail address: alessandramaria.bossi@univr.it (A.M. Bossi).

https://doi.org/10.1016/j.bios.2022.114707
Received 18 May 2022; Received in revised form 13 August 2022; Accepted 6 September 2022
0956-5663/

(Gupta and Verma, 2009; Klantsataya et al., 2017; Martínez-Hernández et al., 2021). Especially, as the portability of the device is a priority for sensors, optical waveguides for SPR sensing enable significative miniaturization and permit to reduce the final costs of the device, thus meeting the requirements posed by in-field measurements (Agrawal et al., 2020; Arcadio et al., 2021; Cennamo et al., 2019; Huang et al., 2022; Kumar et al., 2021) and by bio-chemical sensing (Wang and Wolfbeis, 2020). Optical fibers can be mono- or multi-modal (Personick S., 1983). Considering multi-mode waveguides, these are characterized by a relatively large cross-section of the core, hence light coupling in and out of the structure is less critical compared to the single-mode fibers. It results that multi-mode waveguide-based photonic devices are especially suited for mass-market products, such as disposable sensors that can be interrogated by using low-cost light sources and spectrometers, including flashlight and camera electronics of smartphones (Bremer and Roth, 2015).

Lately, the plasmonic performances have been enhanced by governing the metal shape, such as exploiting metal nanoparticles, or nanostructures, so to modify the description of the interface between the nanostructure and the local dielectric environment (Cennamo et al., 2021a; Jain et al., 2008; Liz-Marzán, 2006). Notable effects on the plasmon originate from the particle morphology, that when deviates from sphericity, as in the case of gold nanostars, both corner sharpness and shape symmetry drive to the intensification of electromagnetic fields near the nanostructure's metal surface, yielding to significative sensitivity enhancements (Burda et al., 2005; Cennamo et al., 2015a; Chatterjee et al., 2021).

The present work explores an innovative geometry for an SPR sensor, based on a spoon-shaped polystyrene optical multi-mode waveguide. The extra-ordinary geometry of this waveguide (Fig. 1) allows to identify two distinctive sensing regions: a first one on the neck of the spoon-shaped waveguide, assimilated to a planar polymer waveguide, and a second one consisting of the concave structure, i.e. the bowl, characterized by angled faces (Fig. 1). Initially, the capability of the spoon-shaped waveguide to perform as a sensing platform was proven by assembling and testing it in three distinctive sensor configurations. Bulk Sensitivity (S_n) and Full Width at Half Maximum (FWHM) were experimentally obtained for all the proposed configurations. Next, the neck planar area and the concave bowl structure of the SPR spoon-shaped waveguide were functionalized with dissimilar receptors, yet specific for the same model analyte, i.e. the protein human serum albumin (HSA). With the aim to study the analytical performances of the distinct sensing areas (i.e. neck and bowl) and to eventually exploit the spoon-shaped waveguide for devising multi-sensing, the bowl was functionalized with an anti-albumin antibody, whereas the neck with albumin-selective molecularly imprinted nanoparticles (nanoMIPs) (Arcadio et al., 2022; Chiappini et al., 2020; Yılmaz et al., 2017). Antibodies are widespread-used high-affinity receptors, with reported dissociation constants and limits of detection for their targets in the nM to pM. NanoMIPs are biomimetic synthetic polymeric receptors prepared by a template assisted synthesis (Arshady and Mosbach, 1981), often referred to as plastic antibodies (Haupt, K. 2010). NanoMIPs can be imprinted with a large variety of chemically and structurally different molecules, hence nanoMIPs can be made to bind the desired target analyte specifically and selectively, while offering several advantages with respect to natural receptors, such as competitive costs, stability to harsh conditions and temperatures, remarkably long shelf-life (Refaat et al., 2019). Moreover, MIPs and nanoMIPs are successfully integrated to a variety of optical sensing platforms (Chiappini et al., 2020). Worth of note is that sensing based on nanoMIPs has been reported to achieve ultralow detection limits, such as the femtomolar (Cennamo et al., 2020; Crapnell et al., 2019; Shrivastav et al., 2017; Çimen et al., 2022). With the aim to study the spoon-shaped waveguide plasmonic probe, state-of-art immuno- and nanoMIP-receptors, targeting the model analyte HSA, were used. It is anticipated that balancing receptors and sensing areas would enable to modulate the biosensor's performance, ultimately allowing to achieve the determination of analytes on distinct sensitivity scales, including when the concentrations are far apart one to the other of several (about eight) order of magnitudes.

2. Experimentals

2.1. Chemicals

All chemicals were from Merck-Sigma (Darmstadt, Germany). Spoon-shaped waveguide was extruded polystyrene (RI = 1.59 @ 600 nm) Art. 270101020 supplied by Italia Soft s.r.l. (Italy). Details in Supplementary Files.

2.2. Interrogation setup

The analysis setup for the specific waveguide was assembled and designed to test three different interrogation modalities. The setup consisted of a halogen lamp, as the white light source (HL-2000LL, Ocean Optics, Dunedin, FL, USA), a spectrometer (FLAME-S-VIS-NIR-ES, Ocean Optics, Dunedin, FL, USA), the SPR spoon-shaped waveguide platform, and plastic optical fibers (POFs) patches (⌀ = 1 mm). For the final assembly, the SPR spoon-shaped waveguide sensor was connected to two similar white light sources and two spectrometers by POFs *via* a custom 3D-printed holder (Supplementary Files). The multisensor was interrogated by dropping the sample on the selected sensitive area and alternating the light insertion and collection from the two sensing areas (see Fig. 1C).

2.3. Functionalization of the spoon-shaped optical waveguide with nanoMIP

NanoMIPs to specifically bind albumin were synthesized and used to functionalize the neck of the spoon-shaped waveguides according to the protocol reported in (Cennamo et al., 2020, 2021a). Details provided in Supplementary Files.

2.4. Functionalization of the spoon-shaped optical waveguide anti-HSA antibody

The anti-albumin functionalization of the angled bowl portion of the spoon shaped waveguide was according to coupling chemistry (Pasquardini et al., 2021), details in Supplementary Files.

2.5. Tests of configurations optical performance

The optical performance of the SPR spoon-shaped waveguide platforms were tested with water:glycerin solutions (RI in the range 1.332–1.408), detailed in Supplementary Files. The plasmonic phenomena were observed in real-time, by placing alternatively a volume of 100 μL of water:glycerin onto the selected sensing surface. Spectral changes were plotted as a function of RI. Measured parameters were the S_n as defined in Equation (1) (Cennamo et al., 2011):

$$S_n = \frac{\delta \lambda_{res}}{\delta n_s} \left[\frac{nm}{RIU}\right] \quad (1)$$

where $\delta\lambda_{res}$ represents the shift in resonance wavelength caused by a variation of the solution's refractive index (δn_s) at the metal surface and expressed as refractive index unit (RIU). The FWHM value was used to describe the bandwidth of the spectral curve.

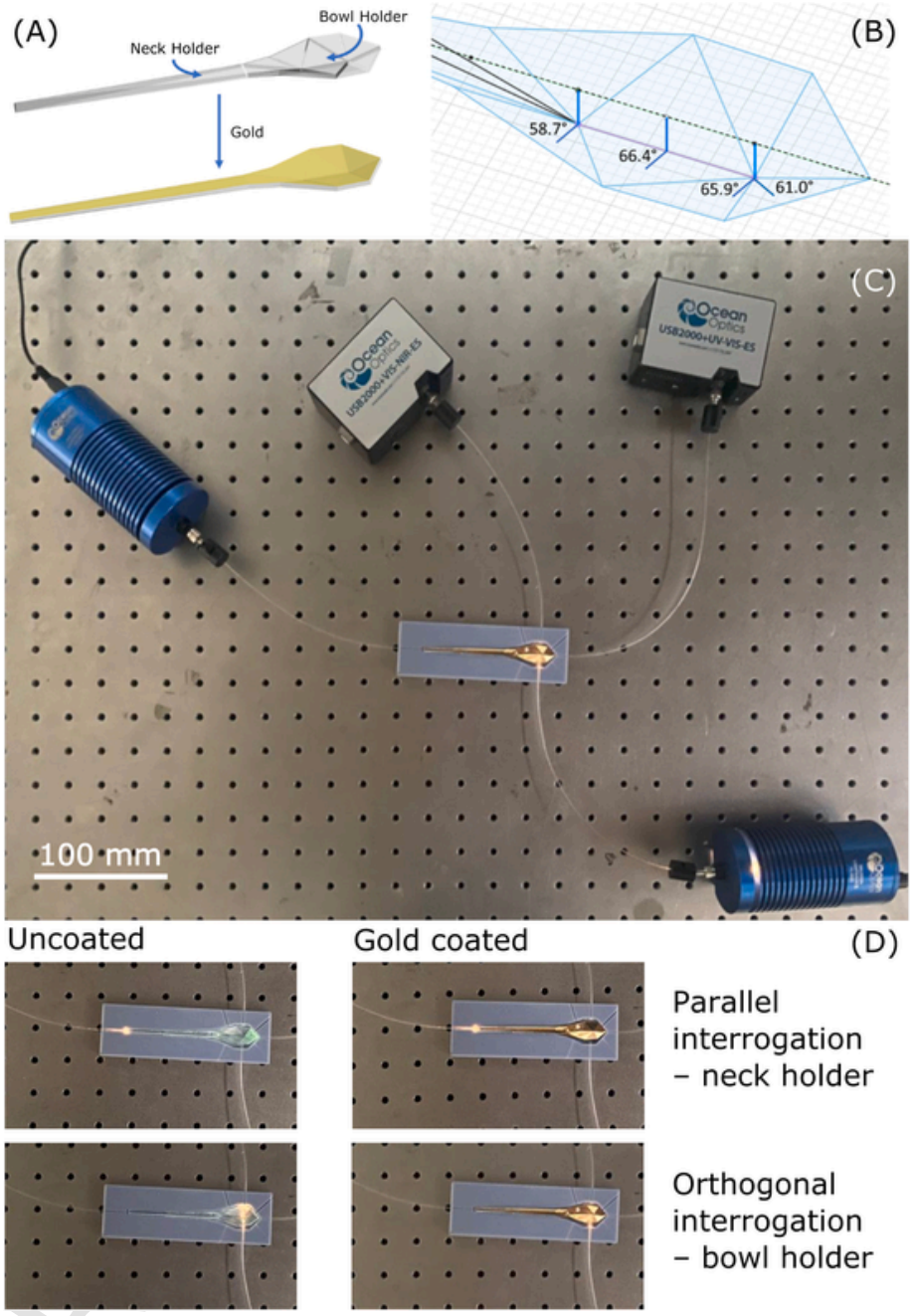

Fig. 1. (A) Geometry of the spoon-shaped optical waveguide. The upper surface of the waveguide was coated with a thin gold layer (~60 nm) to attain the plasmonic phenomenon. (B) Details of the bowl's face angles; the angles of this first example of spoon-shaped waveguide were that of the commercial design. (C) Set-up of the plasmonic sensing platform: two light sources and two spectrophotometers enabled to interrogate the system both parallelly and orthogonally to the spoon's main axis. The readout of the set-ups was obtained by alternatively inserting light on either configuration. (D) The optical guiding effect's changes can be appreciated on the uncoated waveguide as a change in the light scattering (i.e. D, Uncoated upper panel: parallel interrogation = green colour; lower panel: orthogonal interrogation = yellow colour). Light travelling through the gold coated waveguides can be perceived as a shine on the gold-coated waveguide (D, Gold coated).

2.6. Determination of the HSA concentration with the multi-sensor

The sensor was tested for the binding of the target analyte, HSA, by dropping alternatively on the selected sensitive area 100 μL of analyte solution in the concentration range 0.53 fM – 5.30 μM. After 5 min incubation, a PBS washing step was carried out and the spectra were acquired using the blank solution (PBS) as a bulk solution. Data were fitted with the Langmuir model equation considering an averaged single binding site *per* nanoMIP particle (Cennamo et al., 2021a; Çimen et al., 2022) and a 1:1 BSA:antibody binding (Yang D. et al., 2016; Ayawei et al., 2017); the selection of Langmuir was supported by the comparison to the results from Hill model fitting (Supplementary Files):

$$\Delta\lambda_c = \lambda_c - \lambda_0 = \Delta\lambda_{max} \cdot \left(\frac{c}{K + c}\right) \quad (2)$$

$\Delta\lambda_c$ is the variation in resonance wavelength, calculated with respect to the blank, at the analyte concentration c; λ_0 is the resonance wavelength at zero concentration (blank); $\Delta\lambda_{max}$ is $(\lambda_c - \lambda_0)$ at saturation; K is the apparent dissociation constant. Results were the average of n = 3 measurements.

3. Results and discussion

3.1. Optical characterization of the spoon-shaped waveguides

The present work was intended to study the behaviour and therefore to define niches of application in plasmonic sensing of an unprecedented polymeric optical waveguide, characterized by a spoon shape, as schematized in Fig. 1. According to the detailed geometry (Fig. 1A), two distinct sensing regions were envisaged on the spoon-shaped waveguide: the neck, that is a shallow planar area (70.0 × 4.5 × 2.0 mm), and the bowl (30.0 × 14.0 × 1.0 mm), characterized by eight angled faces (Fig. 1B), that appear to have peculiar characteristics in scattering the light (Fig. 1D Uncoated), hence were envisaged to have dissimilar capacity of influencing the plasmonic phenomena, alike light diffusing polymer fibers (Arcadio et al., 2022). To achieve the plasmonic phenomenon, the polystyrene spoon-shaped waveguide (RI = 1.59 @ 600 nm, Italia Soft, Italy) was coated with a thin gold film (~60 nm) by means of a metal sputtering deposition (details in Supplementary Files) (Sultanova et al., 2009).

Neck and bowl of the spoon-shaped waveguide were both considered sensitive areas suitable for optical interrogation. The plasmonic responses were explored testing the spoon-shaped waveguide in different optical configurations (Figs. 1C and 2). The tested configurations were named according to both the selected sensitive area (neck/bowl) and the directions of the light launched in and collected from the main length of the waveguide (parallel/orthogonal).

As reported in Fig. 2A, "Parallel interrogation – neck holder" was characterized by the neck, planar region of the SPR spoon-shaped waveguide sensor sensitive surface and a parallel insertion and collection of light. Exploiting the same parallel interrogation geometry, but using, as sensing area, the concave part of the spoon-shaped waveguide, i.e. the bowl, the "Parallel interrogation – bowl holder" configuration was realized (Fig. 2B). Finally, Fig. 2C schematizes the "Orthogonal interrogation – bowl holder", in which the bowl sensitive area, with faces angled (58.7°–66.4°) with respect to the normal to the centre, is interrogated with the light inserted and collected at a 90° angle with respect to the major axis length of the spoon.

As a first step, the optical behaviours of these three configurations were tested placing on the gold-sensing areas water:glycerine (v/v) mixed solutions with refractive indexes (RIs) encompassing the range 1.332–1.408. Fig. 2 (D-F) reports the SPR spectra for each tested RI and plotted as transmitted light normalized to the reference spectrum (using air as the surrounding medium). In all the cases, the resonance wavelength shifted to the red when the RIs of the solutions increased.

The "Parallel interrogation – neck holder" and "Parallel interrogation – bowl holder" showed a quite narrow SPR spectra even for high RI solutions, suggesting that such configurations are suitable to measure specific samples characterized by high RIs, such as transformer oils (Cennamo et al., 2015b). In contrast, "Orthogonal interrogation – bowl holder" showed the broadest SPR spectra, a condition in which the determination of the wavelength shifts becomes uncertain for high RIs, and therefore the sensor's interrogation had to be restricted to lower RI's samples.

To compare the sensor's performances, the S_n and FWHM of the spectra were estimated. The S_n, as *per* Eq. (1), is defined as the resonance wavelength shift ($\partial\lambda$) caused by the unit average RI change (∂n) surrounding the sensing region (Maharana et al., 2014). The magnitude of S_n mainly depends on the overlap integral of the surface plasmon polaritons electric field intensity on the vertical axis in the analytical region (Shalabney and Abdulhalim, 2011). In terms of resonance dip's FWHM, conventional SPR sensors exhibit values of ~100 nm (Maharana et al., 2014). Fig. 3A shows the resonance wavelength shifts ($\Delta\lambda$) for all the tested configurations, calculated with respect to water (n = 1.332), and as a function of RIs. From Eq. (1) the S_n values can be approximated to the first derivative of the quadratic fittings (Fig. 3A). The S_n values, plotted as a function of RIs (Fig. 3B), showed that "Orthogonal interrogation – bowl holder" displayed the highest S_n in the RI range 1.332–1.392. The performance parameters, for the three tested configurations, at the fixed RI value of 1.372 were also considered (Fig. 3B, inset). The S_n values for the "Parallel interrogation – neck holder" and "Orthogonal interrogation – bowl holder" (i.e. 750 and 950 nm/RIU respectively) were superior to "Parallel interrogation – bowl holder", and resulted akin or slightly superior to plasmonics based on specific nanostructured metal surfaces, such as crossed surface relief-

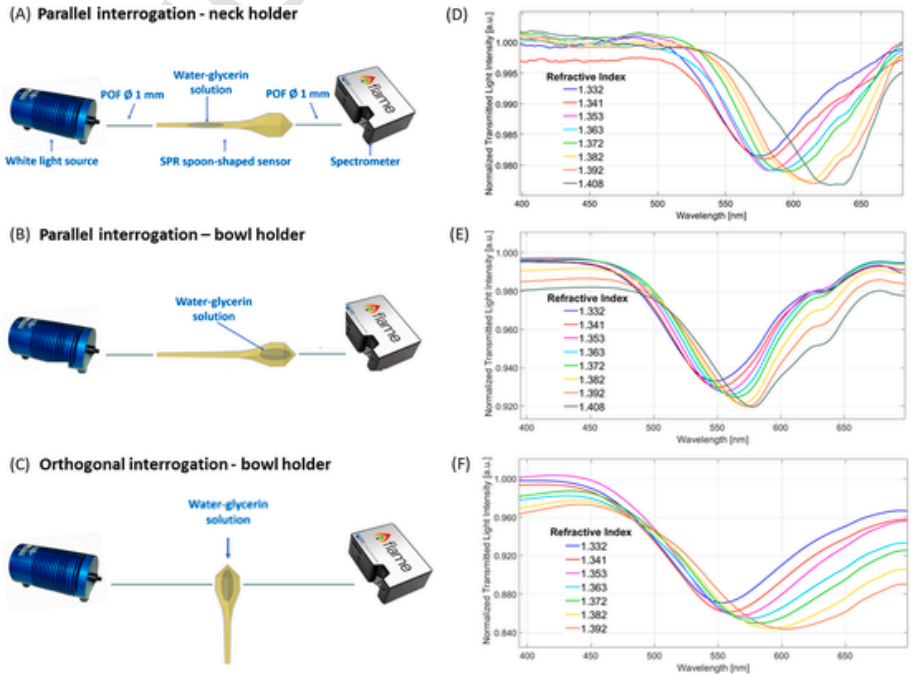

Fig. 2. Experimental SPR sensor configurations based on spoon-shaped polymer waveguides: (A) "Parallel interrogation – neck holder" (B) "Parallel interrogation – bowl holder" and (C) "Orthogonal interrogation – bowl holder" and SPR spectral changes obtained as a function of the variation of RI of water-glycerine solutions, shown in (D), (E) and (F) for the three sensor configurations, respectively.

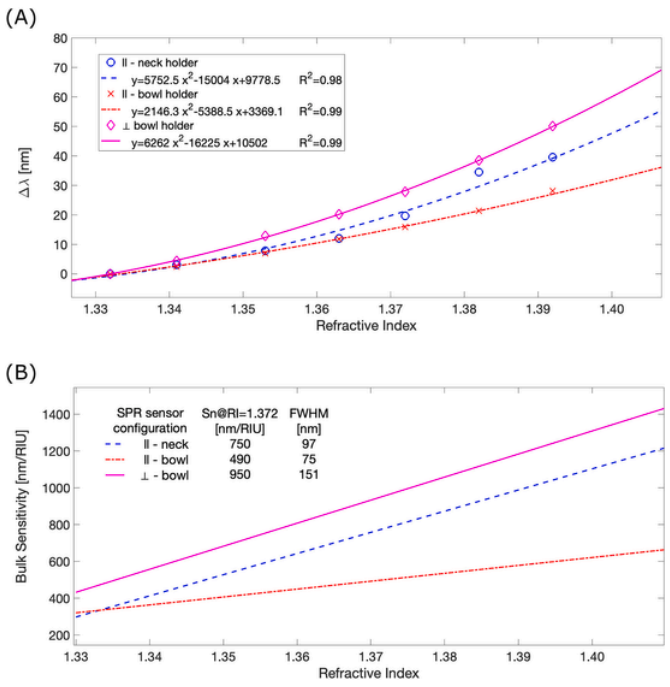

Fig. 3. (A) Resonance wavelength variation (Δλ) *versus* solution's RI and quadratic fitting of the data (lines) for all the tested experimental configurations. Stdv ≤0.4%. (B) S_n as a function of the solution's RIs for the three configurations and comparison of the S_n and FWHM values at RI = 1.372.

gratings (i.e. S_n = 647.8 nm/RIU) (Nair et al., 2017), and nanoparticle-enhanced plasmon on multi-mode optical waveguides (i.e. S_n = 608.6 nm/RIU) (Walter et al., 2020). "Parallel interrogation – neck holder" (i.e. S_n = 750 nm/RIU; FWHM = 97 nm) showed parameters comparable to 3D-printed planar waveguides characterized by a core having similar optical characteristics (Cennamo et al., 2021b,c). Thus, "Parallel interrogation – neck holder" was assimilated to a planar polymer waveguide.

Concerning the effects of choosing concave structures as sensitive areas ("Parallel interrogation – bowl holder") with respect to planar ones, the plasmonic phenomenon resulted improved in FWHM value, which decreased of about 23% with respect to the "Parallel configuration – neck holder", but concurrently an S_n loss of ~35% was observed (Fig. 3B inset). Instead, maintaining the concave sensitive area but by changing the way the light was inserted/collected in/from the sensor, i.e. "Orthogonal interrogation – bowl holder", a significant increment in S_n (~27%) was observed concurrently to the worsening in the SPR spectra width (~55% FWHM increment). These results indicated that the plasmonic phenomena can be modulated by introducing angled faces in the waveguide, paving the way to forthcoming waveguides with optimized unconventional geometries.

The trade-off between S_n and FWHM values, a well-known aspect in SPR monomodal sensors (Gasior et al., 2014; Kanso et al., 2008), can be discussed in terms of Figure of Merit (FOM defined as S_n/FWHM), that is a quantitative indicator for characterizing the sensor performance (Rahman et al., 2020). Thus, the FOM for the three configurations were estimated, aware that FOM loses part of its significance when applied to multimode SPR sensors (this case), which are characterized by intrinsically superior sensitivities, with respect to single modes, but in turn by worse FWHM figures. The FOM of "Parallel interrogation – neck holder" was 7.7; "Parallel interrogation – bowl holder" had FOM = 6.5 and "Orthogonal interrogation – bowl holder" displayed 6.2. These values were similar to those reported for SPR nanoantennas having non-symmetrical elliptical shapes (FOM = 8.35) (Rahman, B. M. A. 2021). When compared to single mode waveguides (FOMs = 15–20) (Gan et al., 2019), the FOMs for spoon-shaped multi-mode waveguides confirmed to be lower. Nevertheless, key advantage of the spoon-shaped waveguide is the possibility to measure samples in a broader range of RIs (1.33–1.40), offering a far greater flexibility of uses, along with the cheaper set up, in contrast to the more restricted RI ranges reported for single modes and the high costs. As a result, the spoon-shaped waveguide was considered as an open optical SPR platform, which can be interrogated *via* different sensing regions and configurations, so to obtain the required trade-off between sensitivity and FWHM. Moreover, plasmonic-response can be tuned by simply varying the interrogated sensitive area (neck *vs*. bowl) and/or the way the light was inserted/collected to/from the SPR sensor (parallel *vs*. orthogonal).

3.2. Biosensors based on the spoon-shaped optical waveguide: effects of multiple optical configurations to sense for human serum albumin

The optical behaviour observed for the neck and the bowl sensing areas, when tested with water–glycerine solutions (RI 1.332–1.408), demonstrated that the spoon-shaped waveguide possesses two distinct bulk sensitivities (Section 3.1). This was instrumental for the implementation of a bio/sensing platform based on the spoon-shaped waveguide. Indeed, in plasmonic sensing, the sensitivity at binding ($S_{binding}$) is given by the following equation (Homola, J. 2003):

$$S_{binding} = (S_1 * S_2) * E \quad (3)$$

It means that $S_{binding}$ is given by the contribution of two components: the sensitivity to the changes in RI produced by the binding of the analyte to the receptor at the sensor surface $(S_1 * S_2)$ and the efficiency (E) at which the presence of an analyte, at a concentration c, is converted into an RI change. (E) depends on the properties of both the receptor and the analyte. Instead, the RI sensitivity depends on two aspects: (S_1) related to the modulation method and the method of excitation of the surface plasma wave (SPW), which also is impacted by the waveguide's geometrical characteristics, and (S_2) that describes the sensitivity of the SPW's propagation constant to the RI change. In view of Eq. (3), the optical responses of neck and bowl sensing areas (Section 3.1) highlight two distinct $(S_1 * S_2)$ values for a same spoon-platform. This emerges as a distinctive property of the spoon-shaped waveguide and let foresee innovative solutions in sensing.

To explore the effect of a sensing platform displaying a pair of $(S_1 * S_2)$ values, the biosensor's setup combined "Parallel interrogation – neck holder" and "Orthogonal interrogation – bowl holder" (Fig. 1D) and an alternate readout. The study of the performances of the two biosensing areas was conducted using HSA as a standard analyte (Cennamo et al., 2021c; Chopra et al., 2021). The neck and bowl sensing regions were functionalized with two different HSA receptors (details in Supplementary Files). Specifically, the planar neck region, characterized by a lower S_n, was functionalized with soft nanoMIPs, which were earlier demonstrated to produce a notable sensitivity gain in the binding tests, hence a great impact on the E term, due to their deformation at binding (Cennamo et al., 2020). On the opposite, the concave bowl area, characterized by the highest S_n, was functionalized with an anti-albumin antibody, that is a less performing receptor (lower E, i.e. lower efficiency of conversions of the presence of analyte at a concentration c into an RI change), when compared to nanoMIPs.

Atomic force microscopy was used to confirm the functionalization of the sensors. The images in Fig. 4 pointed out marked morphological differences for the nanoMIP functionalized area with respect to the antibody area. The nanoMIPs yielded to a fairly uniform layer of spherical nanoparticles characterized by a mean diameter of 30 ± 4 nm calculated from grain analysis (dry state), consistent with the value of the hydrodynamic diameter in solution estimated from Dynamic Light Scattering (i.e. Z_{ave} ~42 nm, Supplementary Files). The antibody functionalized area showed a non-structured topography, characterized by surface roughness due to antibodies and proteins residuals.

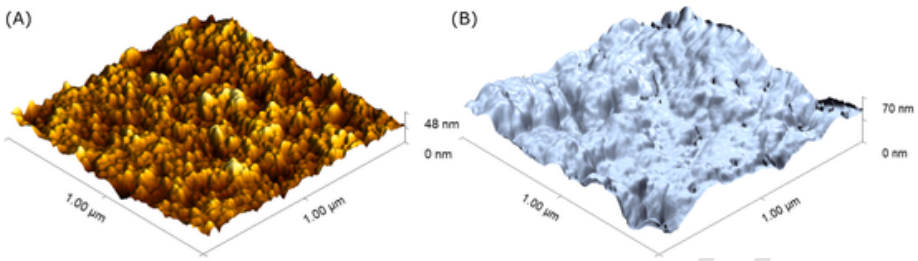

Fig. 4. Atomic force microscopy 3D-view of the surface topography of: (A) nanoMIP's functionalized sensing area; (B) antibody functionalized sensing area. Details of data analysis in SI; data analysis software Gwyddion (Nečas and Klapetek, 2012).

The performances of the two biosensing regions were tested with increasing concentrations of HSA. The sample (100 µL) was alternatively placed on each sensing area, ensuring the thickness of the sample-solution layer greatly exceeded the penetration field (≤1000 nm) and thus restricting the plasmonic phenomena to the binding events.

The antibody-based "Orthogonal interrogation – bowl holder" biosensor was tested with HSA concentrations ranging from 0.53 to 5300 nM, thus encompassing a typical concentration interval for immune-receptor combined to SPR probes (Chopra et al., 2021). As shown in Fig. 5A, the resonance wavelength shifted toward higher values (red-shift), when the analyte concentration increased. Fig. 5B reports the binding isotherm for the immuno-sensor together with the Langmuir model fitting (details in Supplementary Files). Next, the "Parallel interrogation – neck holder" configuration functionalized with nanoMIPs was tested, choosing the HSA detection interval from previously implemented nanoMIPs-plasmonic sensors, in which nanoMIPs were reported to attain femtomolar limits of detection (Cennamo et al., 2020, 2021a). Fig. 5C reports the SPR spectra obtained by this sensor configuration at different HSA concentrations ranging from 5.3 fM to 530 fM. It was observed that for the nanoMIP-biosensor, increasing the HSA concentration corresponds to resonance wavelength shifts toward lower values (blue-shift). Such a peculiar behavior is explained by the deformation of the nanoMIPs at binding, as earlier reported (Cennamo et al., 2020, 2021a). Fig. 5D reports the absolute value of the resonance wavelength variation versus the HSA concentration and the Langmuir fitting. Table 1 draws a comparison between the binding parameters, estimated by the Langmuir model, of the immuno-sensing area and the nanoMIP-sensing one.

The apparent dissociation constant, K, can be considered as an indicator quantitatively correlated to the $S_{binding}$ for a defined sensing area. Table 1 shows that K for the nanoMIP-sensing was 43 fM while K for the immunosensor was 52 nM. The two values are far apart one each other of 6 orders of magnitude. This not only suggests that the spoon-shaped waveguide can work as a multi-sensor, by exploiting different receptors, but that it has the notable effect to enable the extension of the measurements in a very wide range of analyte concentrations, which is rather uncommon in most sensors. In support, the analytical parameters of the biosensing platform are summarized in Table 2. The linear range for the nanoMIP-sensing area was 15–270 fM; that of the immunosensing-area was 2–785 nM. These results prove that the spoon-shaped waveguide enables sensing over a wide dynamic range of concentrations, namely 8 orders of magnitude when considering the LODs, and this is achieved through a single optical platform characterized by two distinct probes (i.e. neck, bowl).

Wide dynamic range sensors are strongly demanded for environmental and health-related applications. In particular to tackle illicit pollutants discharges in open waters (Pitt, R. 2004), or to assess the evolution of pandemics by monitoring the situation through the analysis of

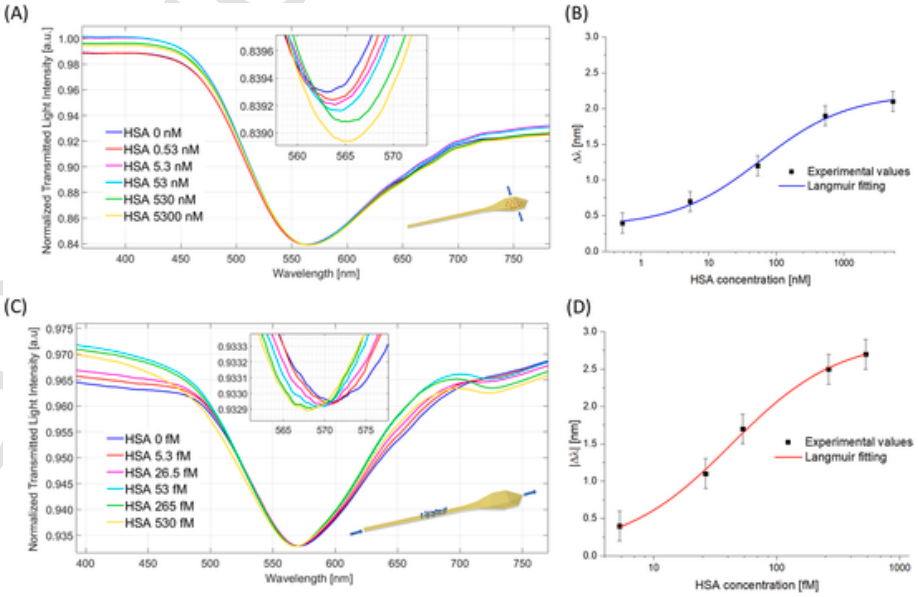

Fig. 5. (A) Plasmonic spectra for "Orthogonal interrogation – bowl holder" with antibody receptor and obtained for HSA concentrations in the range 0.53–5300 nM. Inset: zoom of the resonance area. (B) Value of resonance wavelength variation (|Δλ|) with respect to the blank, plotted as function of HSA concentration (semi-log scale); Langmuir fitting of the experimental values (blue line) and error bars (n = 3). (C) Plasmonic spectra of "Parallel interrogation – neck holder" with nanoMIPs receptor for HSA concentrations in the range 0.53–530 fM. Inset: zoom of the resonance area. (D) Absolute value of resonance wavelength variation (|Δλ|), with respect to the blank, *versus* HSA concentration and Langmuir fitting (red line) of the experimental values and error bars (n = 3).

Table 1
Comparison between the immuno- and nanoMIP-sensing areas.

Parameters	⊥ – bowl immuno-sensor	ll – neck nanoMIP-sensor
$\lvert\Delta\lambda_0\rvert$ [nm]	0.014 ± 0.004	0.073 ± 0.092
$\lvert\Delta\lambda_{max}\rvert$ [nm]	2.213 ± 0.009	2.909 ± 0.066
K [M]	52 ± 22 10^{-9}	43 ± 6 10^{-15}
Reduced χ^2	0.011	0.003
Adj. R^2	0.988	0.996

Table 2
Analytical parameters relative to HSA detection for the two biosensing areas.

Optical configuration & Receptor	Affinity Constant (K_{aff} = 1/K)	Sensitivity at low concentration ($\lvert\Delta\lambda_{max} - \Delta\lambda_0\rvert$/K)	LOD** (3*standard deviation of blank/ sensitivity at low concentration)
⊥ – bowl-antibody	0.019 ± 0.010 nM^{-1}	0.042 nm/nM	0.28 nM
ll – neck-nanoMIP	0.023 ± 0.003 fM^{-1}	0.066 nm/fM	4.16 fM

** from: Thompson et al., (2002).

the sewages in urbanized areas. Moreover, the huge variability of the viral load among patients also requires wide dynamic range sensors (Buckley et al., 2022).

The extension of the dynamic range of measurement of a sensor can be achieved by targeting the (*E*) parameter of Eq. (3). This strategy consists essentially in a chemical approach: it considers that a single-site binding receptor (i.e. a single K value) produces a fixed, hyperbolic dose-response curve, limited in its dynamic range to a fixed 81-fold analyte concentration variation (Vallée-Bélisle et al., 2012; Wei et al., 2018). Therefore, to broaden the dynamic range, a careful mix of n receptors (n ≥ 2) can be exploited, and the chosen receptors have ideally K values (i.e. 1/affinities) far apart one each other of ca. 80-fold. This strategy works well when receptors are nucleic acids, such as molecular beacons and aptamers, whose K values can be programmed through a relatively easy process, which consists of changing the number of mismatched bases, so increasing or decreasing the affinity. Instead, the modulation of K values in other types of receptors, such as antibodies, biomimetics and MIPs, can be less straightforward.

Concerning the MIPs, when functional polymers, such as hydrogels, are imprinted, these have the property to deform at binding with an enhancing impact on $S_{binding}$ (Matsui, J. 2005). This demonstrated true also for soft nanoMIPs receptors, in which the deformation at binding (*E*) played the role to attain very high sensitivities, i.e. attomoles (Cennamo et al., 2020). Yet, the dynamic range of nanoMIPs are restrained by their K value, unless more than a single population of binding site is co-working on the sensors, such as possibly suggested by a thrombin-sensing SPR-nanoMIPs that has a 4 orders of magnitude dynamic range and is characterized by two distinct segments (Çimen et al., 2022). Overall, (*E*) can be modulated through nano/MIPs by mastering the affinity during the syntheses and by conveniently mixing these receptors.

Alternatively, physical options to extend the dynamic range of a sensor implies to act on $(S_1 * S_2)$. Among the examples, tapering to various degrees the optical fibers and/or modifying the thickness of the metal layer both impacts on the overall $(S_1 * S_2)$ term (Chopra et al., 2021). Indeed, tapered optical fiber plasmonic sensing reports dynamic ranges encompassing 1 fM – 100 nM (Liyanage et al., 2021). Finally, the extension of the dynamic range is also being attained by mixed transduction, for example by coupling electrochemistry to LSPR, taking advantage of nanoparticles with ultrasensitivity to RI change (Zhang et al., 2015). Yet, this strategy is powerful, but has the cost of an increased complexity of the device. In contrast, the spoon-shaped waveguide platform provides just a single plasmonic waveguide, which contains distinctive sensitive regions, suitable for a multi-receptor design, so to ultimately meet the required dynamic range.

4. Conclusion

The unprecedented design of a spoon-shaped plasmonic bio/chemical sensor is herein reported. The peculiar geometry of the waveguide is instrumental for innovations in flexible plasmonic platforms, apt to take advantage of the dissimilar sensitivities associated to distinct spoon areas (i.e. neck, bowl). The possibility to tune the plasmonic performance, by changing both the sensing region and the way the light is launched/collected to/from the sensor, was also demonstrated. The combination of two distinct receptors, namely an antibody and a nanoMIP, to functionalize two separate sensing areas, provided a multi-sensor able to attain the detection for HSA encompassing about eight orders of magnitude of concentrations (low fM to hundreds of nM). The remarkable amplitude of the analyte detection range, which is so far uncommon, makes the platform extremely promising. These findings pave the way to study non-usual waveguide geometries and opens to their integration into custom-designed mono- or multi-analyte, multi-range biosensors.

CRediT authorship contribution statement

Nunzio Cennamo : Conceptualization, Methodology, Supervision, Writing – review & editing. **Francesco Arcadio :** Investigation, Data curation, Writing – original draft. **Mimimorena Seggio :** Investigation, Data curation. **Devid Maniglio :** Investigation, Data curation, Writing – review & editing. **Luigi Zeni :** Supervision, Funding acquisition, Writing – review & editing. **Alessandra Maria Bossi :** Conceptualization, Methodology, Supervision, Writing – original draft, Writing – review & editing.

Declaration of competing interest

The authors declare that they have no known competing financial interests or personal relationships that could have appeared to influence the work reported in this paper.

Data availability

Data will be made available on request.

Acknowledgements

NC and LZ acknowledge the VALERE Program of the University of Campania “Luigi Vanvitelli” and the support by EU-ENICBCMED TRANSDAIRY Project. AMB and MS acknowledge the Italian Ministry of University for the Project DM 1062 2021 "Ricercatori a Tempo Determinato di tipo A (RTDA) Azione IV.6 - Contratti di ricerca su tematiche Green” awarded to MS (40-G-15185-5).

Appendix A. Supplementary data

Supplementary data to this article can be found online at https://doi.org/10.1016/j.bios.2022.114707.

References

Agrawal, N., Saha, C., Kumar, C., Singh, R., Zhang, B., Kumar, S., 2020. IEEE Trans. Instrum. Meas. 69, 9097–9104.
Arcadio, F., Zeni, L., Montemurro, D., Eramo, C., Di Ronza, S., Perri, C., D'Agostino, G., Chiaretti, G., Porto, G., Cennamo, N., 2021. Phot. Res. 9, 1397–1408.
Arcadio, F., Seggio, M., Del Prete, D., Buonanno, G., Mendes, J., Coelho, L.C.C., Jorge, P.A.S., Zeni, L., Bossi, A.M., Cennamo, N., 2022. Nanomaterials 12, 1400.
Arshady, R., Mosbach, K., 1981. Makromol. Chem. 182, 687–692.

Ayawei, N., Ebelegi, A.N., Wankasi, D., 2017. J. Chem. 3039817.
Bremer, K., Roth, B., 2015. Opt Express 23, 17179–17184.
Buckley, C., Wang, C.Y., Chatfield, M.D., Bletchly, C., Harris, P., Whiley, D., 2022. Diagnosis microbiol. Infect. Disease 102, 115598.
Burda, C., Chen, X., Narayanan, R., El-Sayed, M.A., 2005. Chem. Rev. 105, 1025–1102.
Cennamo, N., Massarotti, D., Conte, L., Zeni, L., 2011. Sensors 11, 11752–11760.
Cennamo, N., Donà, A., Pallavicini, P., D'Agostino, G., Dacarro, G., Zeni, L., Pesavento, M., 2015a. Sensor. Actuator. B Chem. 208, 291–298.
Cennamo, N., De Maria, L., D'Agostino, G., Zeni, L., Pesavento, M., 2015b. Sensors 15, 8499–8511.
Cennamo, N., Zeni, L., Ricca, E., Isticato, R., Marzullo, V.M., Capo, A., Staiano, M., D'Auria, S., Varriale, A., 2019. Talanta 194, 289–297.
Cennamo, N., Maniglio, D., Tatti, R., Zeni, L., Bossi, A.M., 2020. Biosens. Bioelectron. 156, 112126.
Cennamo, N., Bossi, A.M., Arcadio, F., Maniglio, D., Zeni, L., 2021a. Front. Bioeng. Biotechnol. 9, 801489.
Cennamo, N., Saitta, L., Tosto, C., Arcadio, F., Zeni, L., Fragalà, M.E., Cicala, G., 2021b. Polymers 13, 2518.
Cennamo, N., Arcadio, F., Del Prete, D., Buonanno, G., Minardo, A., Pirozzi, S., Zeni, L., 2021c. IEEE Sensor. J. 21, 16054–16060.
Chatterjee, H., Bardhan, D., Pal, S.K., Yanase, K., Ghosh, S.K., 2021. J. Phys. Chem. Lett. 12, 4697–4705.
Chiappini, A., Pasquardini, L., Bossi, A.M., 2020. Sensors 20, 5069.
Chopra, A., Mohanta, G.C., Das, B., Bhatnagar, R., Pal, S.S., 2021. IEEE Sensor. J. 21, 12153–12161.
Crapnell, R.D., Canfarotta, F., Czulak, J., Johnson, R., Betlem, K., Mecozzi, F., Down, M.P., Eersels, K., Van Grinsven, B., Cleij, T.J., Law, R., Banks, C.E., Peeters, M., 2019. ACS Sens. 4, 2838–2845.
Gan, S.M., Menon, P.S., Mohamad, N.R., Jamil, N.A., Majlis, B.Y., 2019. Mater. Today Proc. 7, 668–674.
Gasior, K., Martynkien, T., Urbanczyk, W., 2014. Appl. Opt. 53, 8167–8174.
Gupta, B.D., Verma, R.K., 2009. J. Sens. 979761.
Haupt, K., 2010. Nat. Mater. 9, 612–614.
Homola, J., 2003. Anal. Bioanal. Chem. 377, 528–539.
Huang, Y., Wang, Y., Xu, G., Rao, X., Zhang, J., Wu, X., Liao, C., Wang, Y., 2022. Biosensors 12, 141.
Jain, P.K., Huang, X., El-Sayed, I.H., El-Sayed, M.A., 2008. Acc. Chem. Res. 41, 1578–1586.
Kanso, M., Cuenot, S., Louarn, G., 2008. Plasmonics 3, 49–57.
Klantsataya, E., Jia, P., Ebendorff-Heidepriem, H., Monro, T.M., François, A., 2017. Sensors 17, 12.
Kretschmann, E., 1971. Z. Phys. 241, 313–324.
Kretschmann, E., Raether, Z, H., 1968. Naturforscher A 23, 2135–2136.
Kumar, S., Singh, R., Yang, Q., Cheng, S., Zhang, B., Kaushik, B.K., 2021. IEEE Sensor. J. 21, 62–70.
Liyanage, T., Lai, M., Slaughter, G., 2021. Anal. Chim. Acta 1169, 338629.
Liz-Marzán, L.M., 2006. Langmuir 22, 32–41.
Maharana, P.K., Jha, R., Palei, S., 2014. Sensor. Actuator. B Chem. 190, 494–501.
Martínez-Hernández, M.E., Rivero, P.J., Goicoechea, J., Arregui, F.J., 2021. Chemosensors 9, 64.
Matsui, J., Akamatsu, K., Hara, N., Miyoshi, D., Nawafune, H., Tamaki, K., Sugimoto, N., 2005. Anal. Chem. 77, 4282–4285.
Mejía-Salazar, Jr, J.R., Oliveira, O.N., 2018. Chem. Rev. 118, 10617–10625.
Nair, S., Escobedo, C., Sabat, R.G., 2017. ACS Sens. 2, 379–385.
Nečas, D., Klapetek, P., 2012. Open Phys. 10, 181–188.
Nguyen, H.H., Park, J., Kang, S., Kim, M., 2015. Sensors 15, 10481–10510.
Pasquardini, L., Cennamo, N., Malleo, G., Vanzetti, L., Zeni, L., Bonamini, D., Salvia, R., Bassi, C., Bossi, A.M., 2021. Sensors 21, 3443.
Personick, S., 1983. IEEE J. Sel. Area. Commun. 1, 373–380.
Pitt, R., 2004. Illicit Discharge Detection and Elimination, A Guidance Manual for Program Development and Technical Assessments. MD: Center for Watershed Protection, US.
Rahman, B.M.A., 2021. Sensors 21, 6166.
Rahman, M.M., Rana, M.M., Rahman, M.S., Anower, M.S., Mollah, M.A., Paul, A.K., 2020. Opt. Mater. 107, 110123.
Refaat, D., Aggour, M.G., Farghali, A.A., Mahajan, R., Wiklander, J.G., Nicholls, I.A., Piletsky, S.A., 2019. Int. J. Mol. Sci. 20, 6304.
Shalabney, A., Abdulhalim, I., 2011. Laser Photon. Rev. 5, 571–606.
Shrivastav, A.M., Usha, S.P., Gupta, B.D., 2017. Biosens. Bioelectron. 90, 516–524.
Singh, P., 2016. Sensor. Actuator. B Chem. 229, 110–130.
Sultanova, N., Kasarova, S., Nikolov, I., 2009. Acta Phys. Pol., A 116, 585–587.
Thompson, M., Ellison, S.L.R., Wood, R., 2002. Pure Appl. Chem. 74, 835–855.
Tong, L., Wei, H., Zhang, S., Xu, H., 2014. Sensors 14, 7959–7973.
Vallée-Bélisle, A., Ricci, F., Planxo, K.W., 2012. J. Am. Chem. Soc. 134, 2876–2879.
Walter, J.-G., Eilers, A., Alwis, L., Roth, B., Bremer, K., 2020. Sensors 20, 2889.
Wang, X., Wolfbeis, O.S., 2020. Anal. Chem. 92, 397–430.
Wei, B., Zhang, J., Ou, X., Lou, X., Xia, F., Vallée-Bélisle, A., 2018. Anal. Chem. 90, 1506–1510.
Yang, D., Singh, A., Wu, H., Kroe-Barrett, R., 2016. Anal. Biochem. 508, 78–96.
Yılmaz, E., Özgür, E., Bereli, N., Türkmen, D., Denizli, A., 2017. Mater. Sci. Eng. C 73, 603–610.
Zhang, D., Lu, Y., Jiang, J., Zhang, Q., Yao, Y., Wang, P., Chen, B., Cheng, Q., Liu, G.L., Liu, Q., 2015. Biosens. Bioelectron. 67, 237–242.
Çimen, D., Bereli, N., Günaydın, S., Denizli, A., 2022. Talanta 246, 123484.